Visual short-term memory related EEG components in a virtual reality setup

Felix Klotzsche, Michael Gaebler, Arno Villringer, Werner Sommer, Vadim Nikulin, & Sven Ohl

Supplementary material

Control analyses

To exclude the possibility that the effects of memory load and eccentricity on the CDA were specific to our selection of the CDA time window (which we gained from the data-driven temporal localizer approach), we conducted a set of supplementary analyses. First, we calculated the mean CDA using the time window reported by Hakim et al. (2019). This alt ernative time window (400 to 1,450 ms after stimulus onset) started (slightly) later and lasted (substantially) longer than the one yielded by the temporal localizer approach (388 to 1,088 ms). In line with our results, we observed also for this alternative time window that the CDA mean amplitude varied significantly with memory load ($F(1,20) = 14.74$, $p = .001$) while stimulus eccentricity did not significantly influence mean CDA amplitude ($F(2,40) = 0.45$, $p = .638$). In contrast to the analysis based on the data-driven time window, there was no significant interaction of eccentricity with the effect of memory load ($F(2,40) = 3.04$, $p = .059$). Post-hoc paired *t*-tests, however, revealed the same pattern as found in the main analysis: the difference between trials with low and high memory load was significant for the eccentricities of 4 dva ($\Delta CDA_{low–high} = 0.47$, 95% CI [0.16, 0.78], $p = .004$) as well as 9 dva ($\Delta CDA_{low–high} = 0.39$, 95% CI [0.16, 0.62], $p = .002$), but not for 14 dva ($\Delta CDA_{low–high} = 0.14$, 95% CI [–0.06, 0.33], $p = .155$). To further explore this pattern with a more sensitive analysis approach, we calculated a hierarchical linear mixed-model (using the statistical software package *lme4*; Bates et al., 2015) which takes single-trial data into account and allows for modeling random intercepts per participant. We modeled the mean CDA amplitude (averaged across channels in our ROI and time points of the respective time window) as a function of memory load (treatment contrast; set size of 2 items as a baseline), eccentricity (treatment contrast; 9 dva as a baseline) as well as their interaction. We fitted one of these models separately for the mean CDA calculated for the time window identified with the temporal localizer method and for the alternative time window, and we determined the significance of the model predictors using the R package lmerTest (Kuznetsova et al., 2017).

This analysis revealed the same pattern of results for both time windows (Table S1): memory load had a strong influence on the mean CDA amplitude while eccentricity did not have a significant main effect. The interaction effect between memory load and eccentricity was small (compared to the main effect of memory load) but significant for both time windows and was driven by the trials with the largest stimulus eccentricity (14 dva) which exhibited a smaller difference between the memory load conditions as compared to trials with 9 dva or 4 dva. There was no significant difference between the two smaller eccentricity conditions. This is the same pattern that we observed with the (non-hierarchical) rmANOVA paired with post-hoc *t*-tests for the data-driven time window. We suspect that we did not observe a significant interaction effect of memory load and eccentricity with the rmANOVA for the a priori time window due to a lack of statistical power. We will discuss in the following paragraph why the interaction effect is smaller in the alternative time window. The more sensitive mixed-model approach allows to detect also weaker effects. Overall, we conclude that the results gained with the original time window (in accordance with the mixed-model) represent a useful while parsimonious description of the data. The key insight: for the largest eccentricity (14 dva), the load effect on the CDA was substantially weakened as compared to the two smaller eccentricities (Figure S1a).

Based on Figure S1a, we assumed that the interaction effect was weaker for the alternative time window as eccentricity might predominantly affect early components of the ERP (like the PNP component). To address this concern, we conducted a time-resolved version of the rmANOVA approach by fitting the according model ($CDA \sim MemoryLoad * Eccentricity$) separately for each sample during the retention interval (Fig. S1b). This revealed different time courses for the main effects of memory load and eccentricity, with the latter peaking substantially earlier, before the onset of the investigated CDA time windows. As expected, the interaction effect only plays a role during the early phases of the CDA time windows and wears of quickly. By using a longer (and/or later) time window to calculate the mean CDA amplitude, the proportion of samples affected by the interaction effect decreases. As the main effect of memory load is stronger and more long lasting, it can also be found more easily in such longer time windows. The post-hoc t-tests, however, did not show differences in CDA mean amplitude for either of the time windows, suggesting that increasing the length of the interval is not sufficient to counteract the effect of the interaction.

Supplementary figures & tables

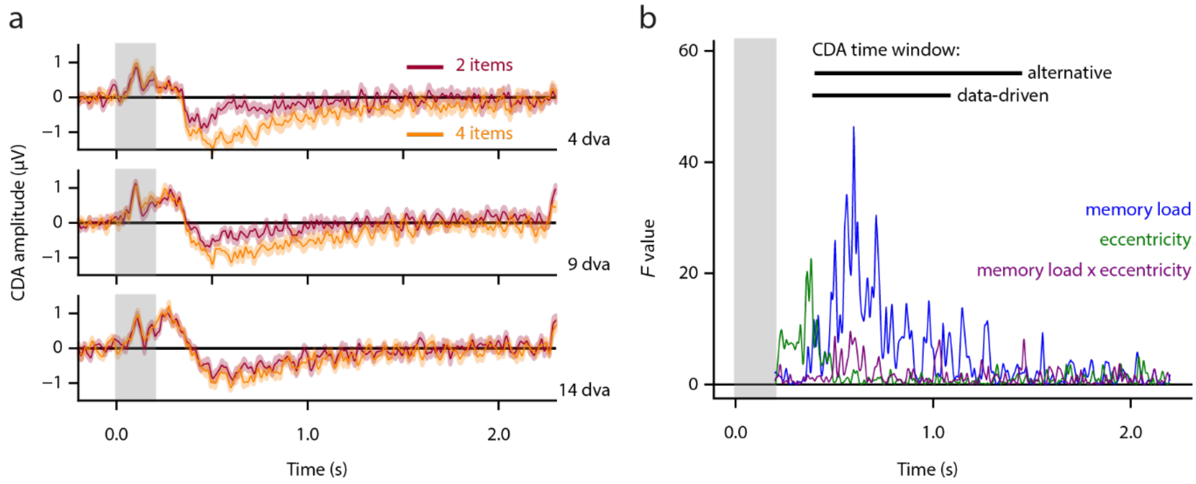

Figure S1: (a) The effect of memory load (2 vs 4 items) on the CDA per eccentricity level. (b) Effects of a time-resolved rmANOVA, modelling the CDA (i.e., lateralized ERP in our ROI) as a function of memory load, eccentricity, and their interaction. It is important to stress the exploratory nature of this supplementary analysis. Therefore, we refrained from performing significance tests.

Table S1

Effects in the mixed-model analysis of the mean CDA amplitude for two different time windows

	predictor	b	*t*	df	95% CI
CDA time window: 388 – 1088ms	Intercept (2 items; 9 dva)	–0.26	–1.87	34.81	[–0.55; 0.02]
	Memory load (4 vs 2 items)	–0.50	–4.73***	13358.30	[–0.71; –0.29]
	Eccentricity (4 vs 9 dva)	–0.05	–0.45	13358.48	[–0.26; 0.16]
	Eccentricity (14 vs 9 dva)	–0.19	–1.77	13358.38	[–0.39; 0.02]
	Memory load x Eccentricity (4 vs 2 items) x (4 vs 9 dva)	–0.08	–0.54	13358.48	[–0.38; 0.22]
	Memory load x Eccentricity (4 vs 2 items) x (14 vs 9 dva)	0.35	2.37*	13358.37	[0.06; 0.65]
CDA time window: 400 – 1450ms	Intercept (2 items; 9 dva)	–0.17	–1.28	38.38	[–0.44; 0.10]
	Memory load (4 vs 2 items)	–0.44	–4.08***	13358.33	[–0.66; –0.23]
	Eccentricity (4 vs 9 dva)	–0.04	–0.36	13358.55	[–0.25; 0.17]
	Eccentricity (14 vs 9 dva)	–0.19	–1.72	13358.42	[–0.40; 0.03]
	Memory load x Eccentricity (4 vs 2 items) x (4 vs 9 dva)	–0.04	–0.26	13358.55	[–0.34; 0.26]
	Memory load x Eccentricity (4 vs 2 items) x (14 vs 9 dva)	0.32	2.12*	13358.42	[0.02; 0.62]

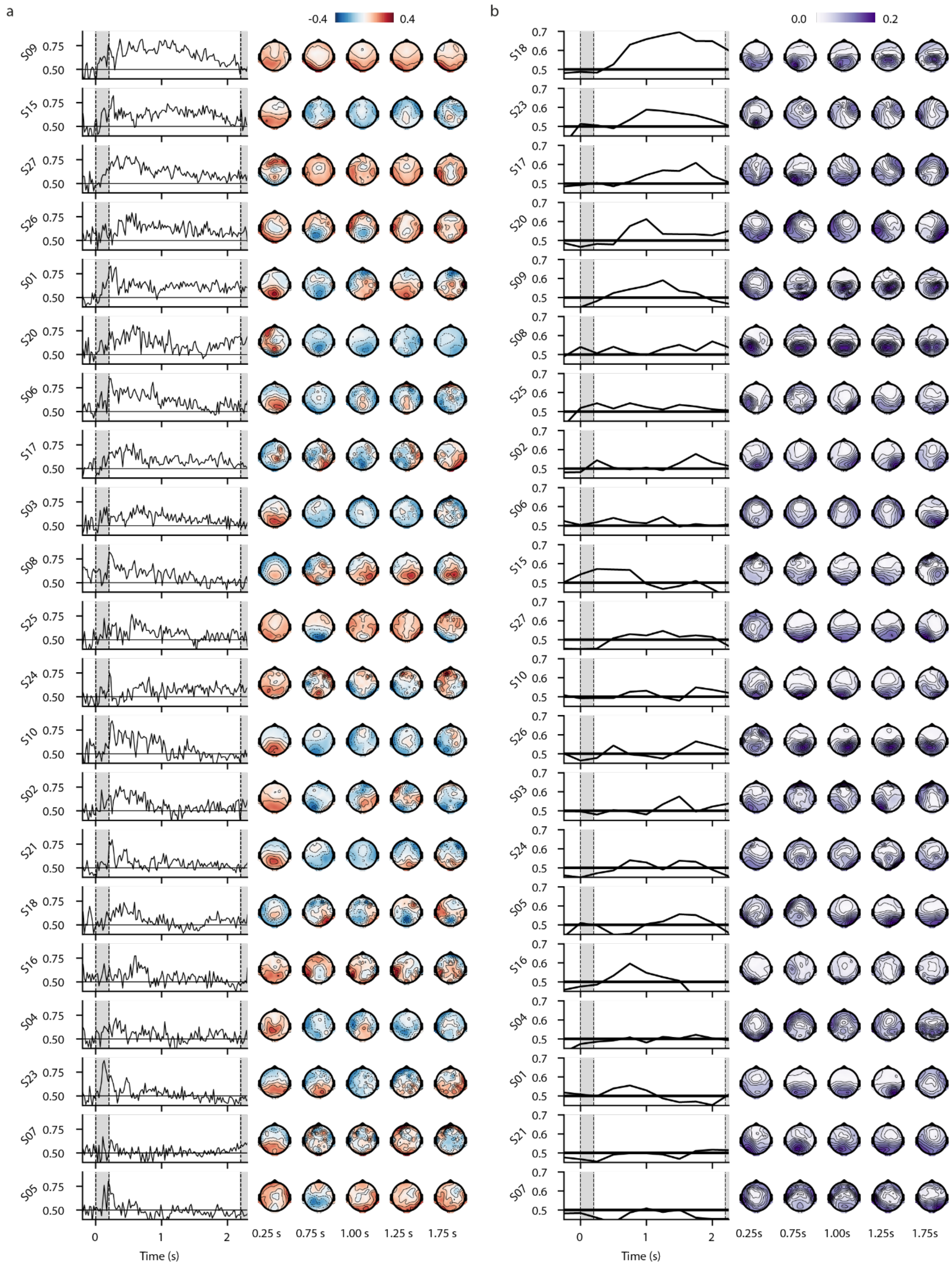
a
-0.4
0.4
b
0.0
0.2
S09 S15 S27 S26 S01 S20 S06 S17 S03 S08 S25 S24 S10 S02 S21 S18 S16 S04 S23 S07 S05
S18 S23 S17 S20 S09 S08 S25 S02 S06 S15 S27 S10 S26 S03 S24 S05 S16 S04 S01 S21 S07
Time (s)
0.25 s
0.75 s
1.00 s
1.25 s
1.75 s
Time (s)
0.25s
0.75s
1.00s
1.25s
1.75s

Figure S2: Time courses of the decoding performance and the associated spatial patterns for the single participants. Participants are sorted, separately for each subfigure, decreasingly by the maximum average decoding performance in the time window in which the overall decoding performance (across participants) was significantly above chance level. (a) Decoding from the broadband EEG data (ERP). (b) Decoding from time-frequency data (here: alpha frequencies 8–14 Hz). As we analyzed induced power, which reflects the non-phase locked signal from an oscillating dipole (i.e., with arbitrary polarity at a given point in time), we show the absolute pattern weights to avoid cancellation across participants and repetitions.

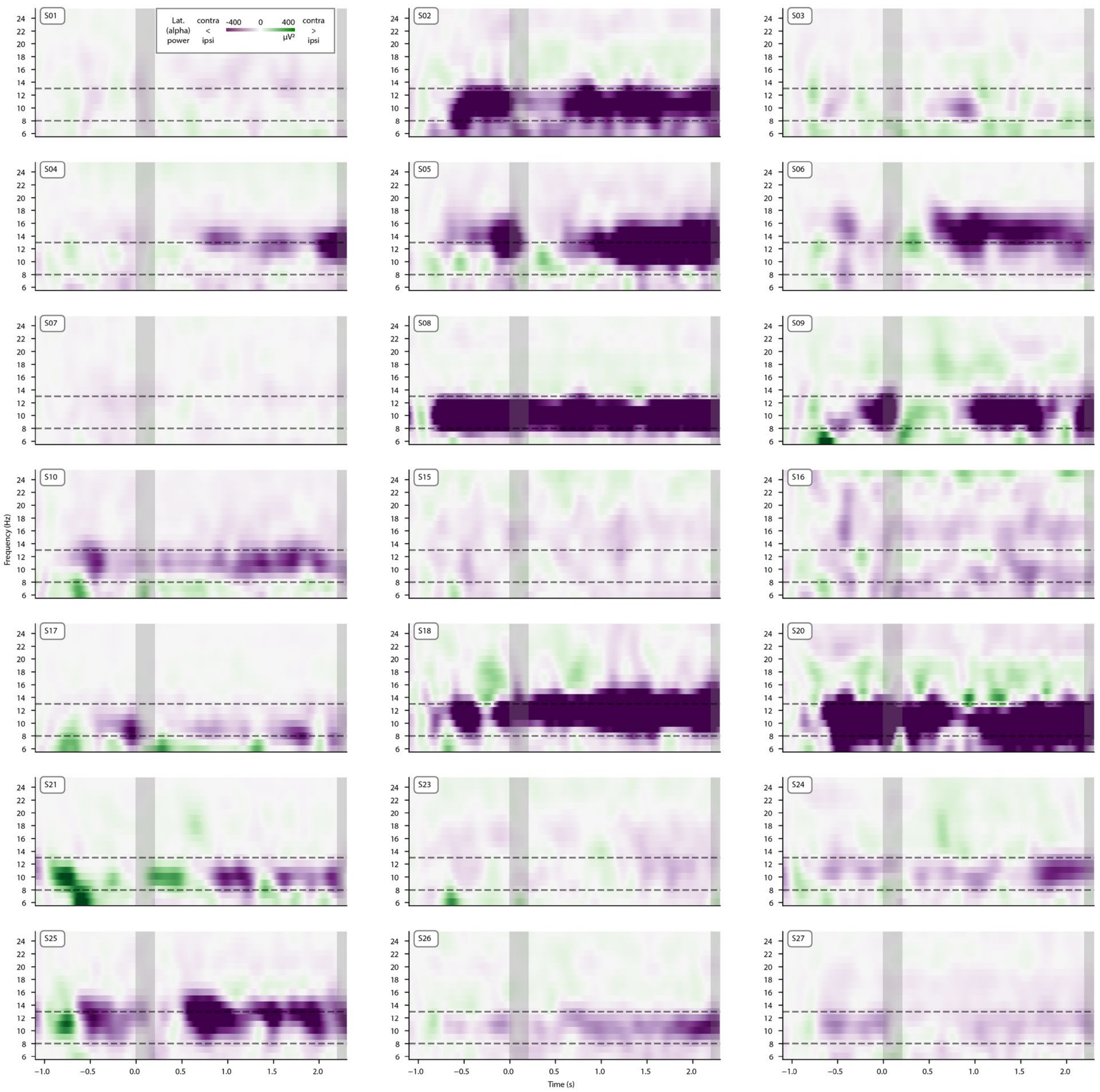

Figure S3: Lateralized time-frequency data (difference between contra- and ipsilateral channels) for each participant. The dotted lines mark the lower and upper limit for the frequency range that we included in our analyses regarding alpha lateralization.

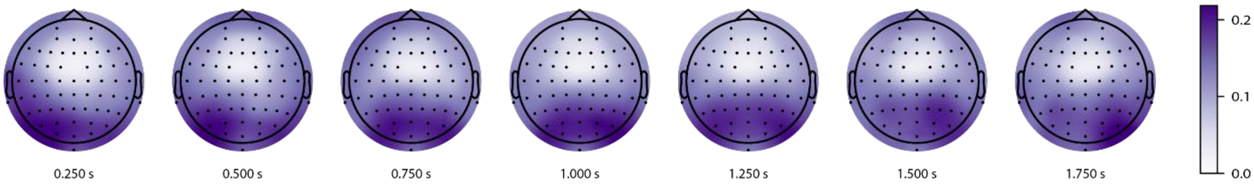

Figure S4: Averaged absolute pattern weights (gained by multiplying the covariance of the EEG data with the filter weights; Haufe et al., 2014) of the most discriminative CSP component (normalized per time-bin and participant before averaging) for the alpha range. As we analyzed induced power, which reflects the non-phase locked signal from an oscillating dipole (i.e., with arbitrary polarity at a given point in time), we show the absolute pattern weights to avoid cancellation across participants and repetitions.

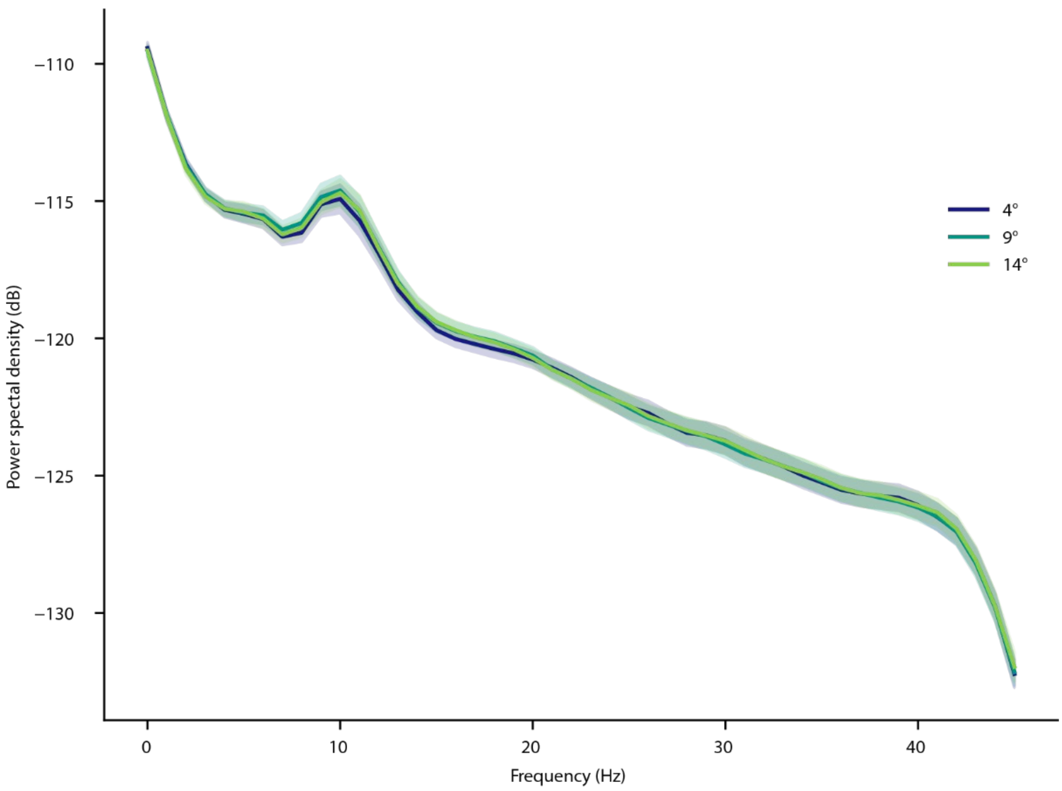

Figure S5: Power spectral density (PSD) per eccentricity condition during the retention interval (shaded area: standard error). Data stems from the bilateral channel-pairs which formed the ROI for the calculation of the CDA and lateralized alpha power. We used Welch's method to calculate the PSD with a window size of 512 samples. An alpha peak is recognizable for each of the eccentricity conditions with no evident difference between the conditions.

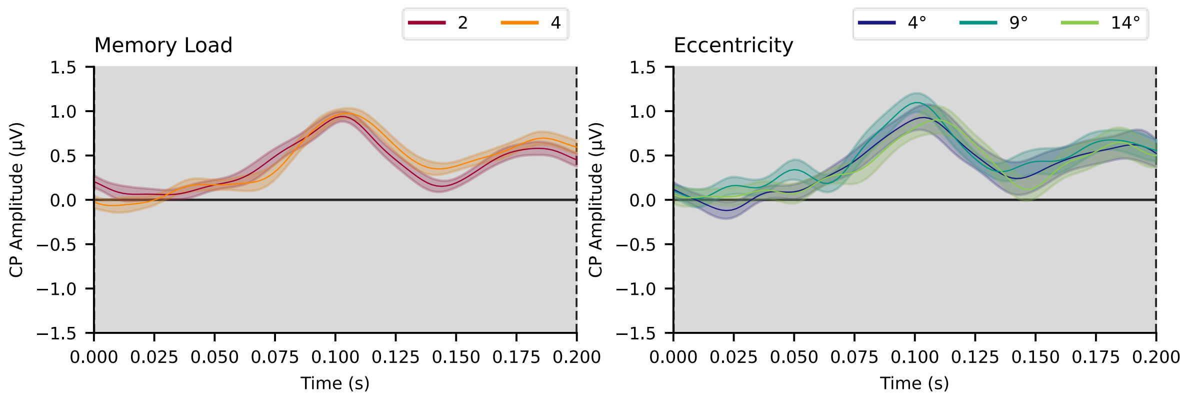

Figure S6: Early contralateral positivity (zoomed-in version of Figure 2a–b). This early potential might have been caused by the offset of the asymmetric, arrow-shaped cue which indicated the relevant hemifield (at time 0, i.e., at the onset of the memory arrays) or indicate enhanced processing of the stimuli in the cued hemifield (Livingstone et al., 2017). Since in our paradigm, the offset of the cue and the onset of the memory arrays coincided, it is not possible to clearly determine the underlying cause of this lateralized potential. However, since it was not modulated by memory load (in contrast to the CDA) or eccentricity of the memory stimuli (in contrast to the immediately following PNP component), it is unlikely that its occurrence influenced the effects of primary interest.

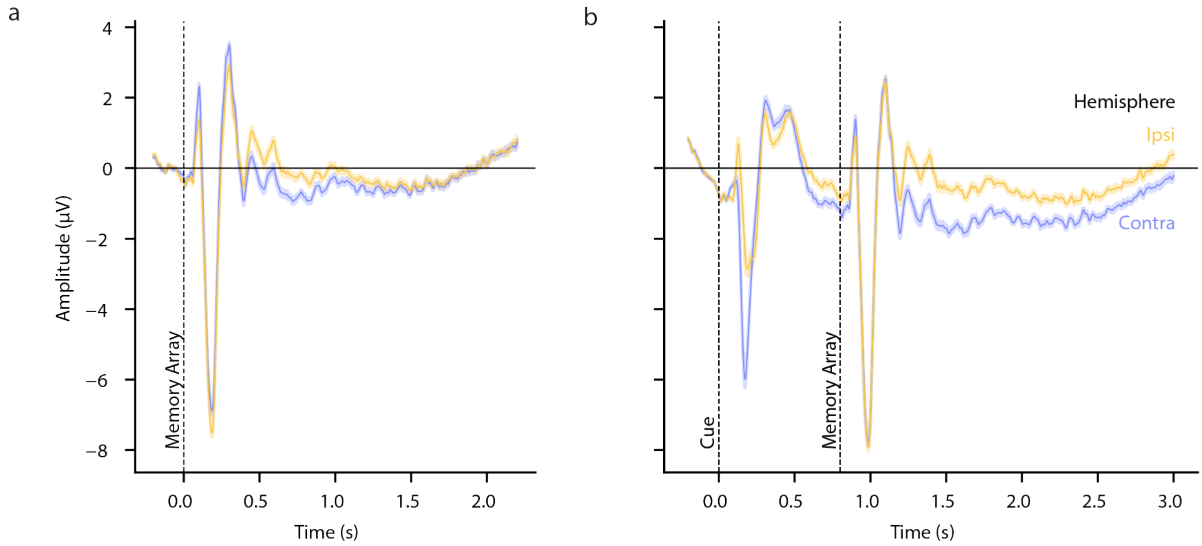

Figure S7: Event-related potential (ERP) for the hemispheres contra- and ipsilateral to the cued array (shaded areas: ±1 SEM corrected for the within-participant measurements). We computed the average signals from channels that were within the same region-of-interest as those used in the analysis of the CDA (P3/4, P5/6, PO3/4, PO7/8, O1/2). **(a)** The event-related potential (ERP) time-locked to memory array onset and normalized by subtracting, on a single-trial basis, the mean amplitude during a 200 ms baseline period prior to this onset. The analyses regarding the CDA as well as the ERP-based decoding analyses were conducted on data in this format. **(b)** ERP time-locked to the onset of the cue (800 ms before onset of the memory stimulus), with the baseline window being shifted accordingly (i.e., 200 ms before the onset of the cue). The CDA effect is discernible in both plots. Additionally, the asymmetric cue induced a lateralized response with a strong positivity during early components (P1, N1), but also another more long-lasting positivity during later stages of the period between cue and memory array onset (i.e., around 500–800 ms after cue onset). This period covers the baseline-window chosen for the epochs time-locked to the onset of the memory array (which formed the basis for our ERP analyses). Therefore, by subtracting the mean activity in this time-window, we may have introduced an artificial lateralization during the rest of the ERP. However, this bias would yield a polarity opposite to that of the CDA. Therefore, such a correction would at most complicate the observation of a CDA, which in turn emphasizes our result that we were able to detect a CDA for all eccentricities. Furthermore, this effect on the baseline-window was (as it occurred before the onset of the relevant stimuli) independent of the experimental manipulations (memory load, eccentricity) and hence impacted all conditions in the same way (i.e., like adding a lateralized constant). Thus, we can rule out concerns of biases in the analysis pipeline as a source underlying our results regarding the CDA or decoding analyses. Finally, we believe that the observed lateralization in the later parts of the cue interval is a concomitant of the spatial shift of attention in response to the cue (Keefe & Störmer, 2021) and is therefore likely to occur in any paradigm which implements spatial cuing preceding the relevant stimulus. Presumably, this effect was also present in various previous studies which used comparable experimental designs/timings. We do not conclude that this is problematic; rather it increases the comparability and compatibility of our findings with previous reports.

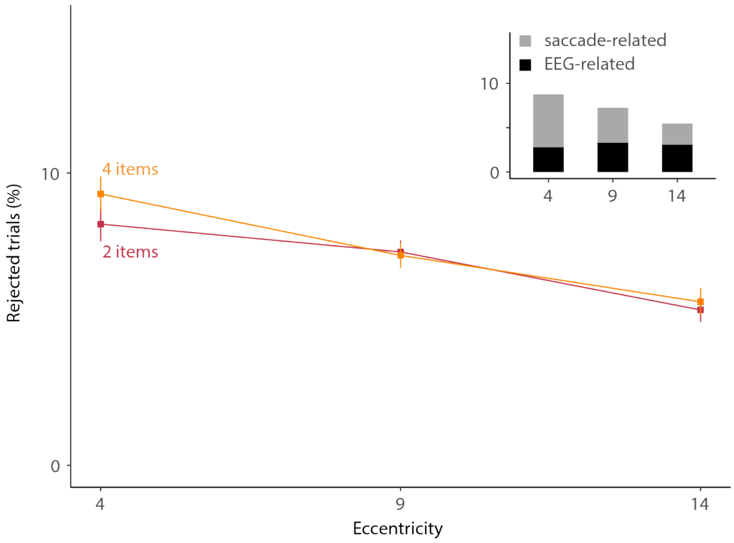

Figure S8: Average proportion of rejected trials per eccentricity for the ERP analysis. We rejected trials which contained saccades with an amplitude of at least 2 dva or were classified as noisy by the cross-validation based trial classification algorithm *autoreject* (Jas et al., 2017). A rmANOVA identified a significant main effect of eccentricity ($F(2,40) = 8.49$, $p = .001$) while neither memory load ($F(1,20) = 0.61$, $p = .443$) nor its interaction with eccentricity ($F(2,40) = 0.61$, $p = .550$) significantly influenced the proportion of rejected trials. Post-hoc *t*-tests corroborated that in the largest eccentricity condition significantly less trials were rejected than for 4 dva ($\Delta_{4\text{–}14} = 3.31\%$, 95% CI [1.33, 5.30], $t(20) = 3.48$, $p = .002$) as well as for 9 dva eccentricity ($\Delta_{9\text{–}14} = 1.79\%$, 95% CI [0.46, 3.11], $t(20) = 2.82$, $p = .011$). There was no difference between the two smaller eccentricities ($\Delta_{4\text{–}9} = 1.53\%$, 95% CI [-0.13, 3.19], $t(20) = 1.92$, $p = .070$). Overall, the differences in the number of rejected trials per condition were rather small. The inset plot shows that the decrease of rejected trials for the largest eccentricity was the consequence of a smaller number of trials that contained saccades in the 14 dva eccentricity condition. We suspect that in conditions with smaller eccentricities, there were more saccadic eye movements, as it is more difficult to suppress reflexive eye movements to task-relevant stimuli that are located close to the current fixation point. This resulted in a larger number of involuntary eye movements in these conditions. Regarding the condition with the highest eccentricity, we excluded the smallest number of trials. Therefore, the absence of a significant memory load effect in this condition cannot be attributed to reduced statistical power resulting from a smaller number of trials compared to the other eccentricities.

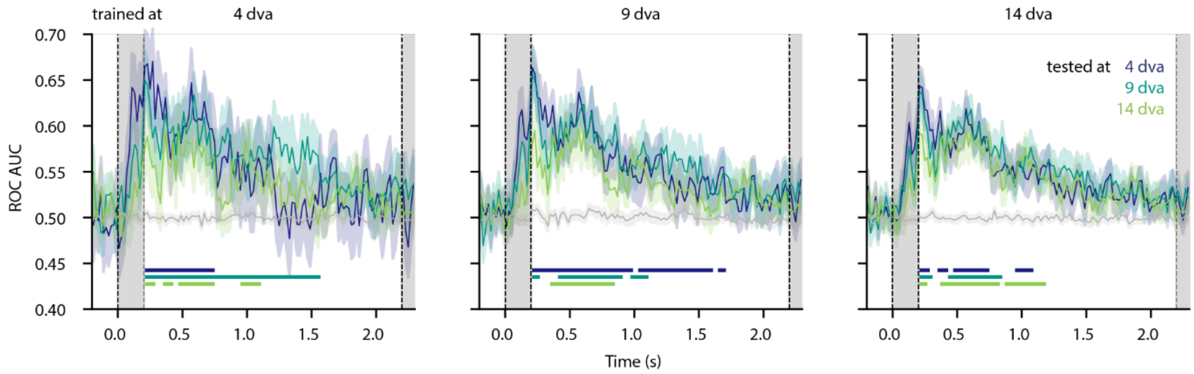

Figure S9: Results of the cross-decoding analysis for the broadband ERP data. To test whether the spatial features of the decoding of memory load are substantially different, we trained different classifiers separately on (80% of) the data from the three eccentricity conditions (see three separate panels). We then tested each of these classifiers either on the remaining data of the same eccentricity condition or on 20% of the data from each of the other conditions. The specific parameters of the classifiers were the same as used in the main decoding analysis on the ERP data (incl. the 100x repeated 5fold cross-validation). The figure shows the time-resolved decoding performance averaged across folds, repetitions, and participants and follows the same conventions as Figure 1f. Classification performance was above chance for each classifier in each condition. However, for none of the classifiers (trained either on data from the 4, 9, or 14 dva condition), we observed significant differences between the performances on the different test sets (as tested by a sliding, cluster-corrected repeated-measures ANOVA).

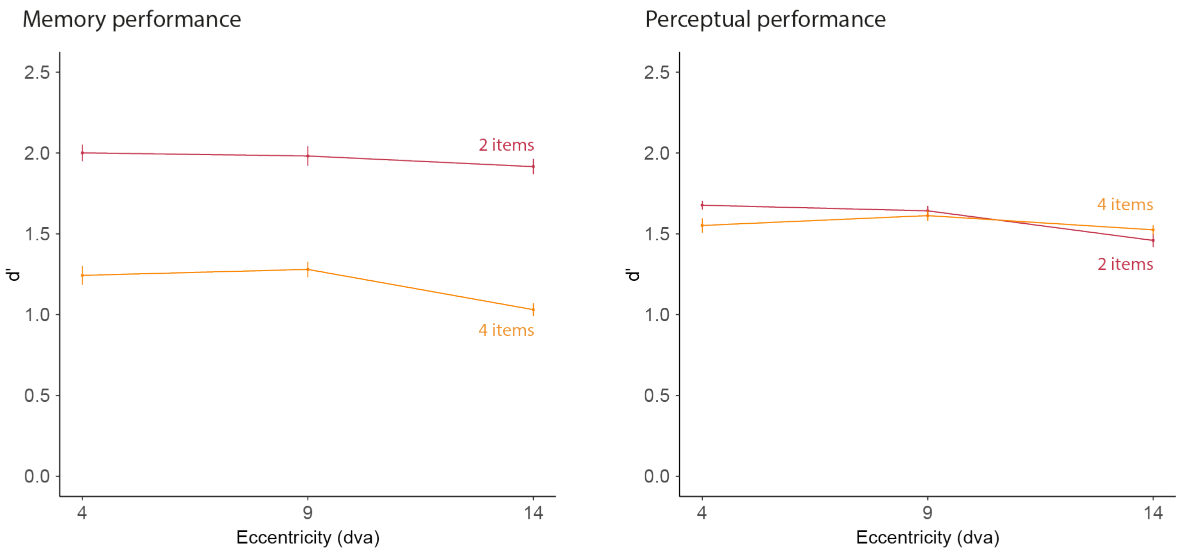

Figure S10: Behavioral results of the memory task and the perceptual task using d' (i.e., sensitivity) as a measure of memory performance. Error bars indicate ±1 SEM, taking into account the repeated measures design (Baguley, 2012; Morey, 2008).

Using d' as a bias-free indicator of memory performance (i.e., sensitivity), we found the same pattern of results as in the analyses using the proportion of correct responses (i.e., accuracy; see Figure 1b-c). In the Memory Task, d' was strongly modulated by memory load and varied only little as a function of eccentricity. Participants showed a significantly higher d' in trials with low (M = 1.97, SD = 0.26, 95% CI [1.89, 2.04]), as compared to high memory load (M = 1.18, SD = 0.35, 95% CI [1.11, 1.26]; $F(1,20) = 114.14$, $p < .001$). The influence of eccentricity was comparatively small but significant ($F(2,40) = 3.88$, $p = .029$). Participants' d' was lowest for the eccentricity of 14 dva (M = 1.47, SD = 0.34, 95% CI [1.40, 1.54]) and significantly lower than for stimuli presented at 9 dva (M = 1.63, SD = 0.28, 95% CI [1.57, 1.69]) or 4 dva (M = 1.62, SD = 0.31, 95% CI [1.56, 1.69]), as corroborated by post-hoc t-tests (Δsensitivity$_{9\text{–}14}$ = 0.16, 95% CI [0.02, 0.29], $t(20) = 2.46$, $p = .023$; Δsensitivity$_{4\text{–}14}$ = 0.15, 95% CI [0.01, 0.29], $t(20) = 2.25$, $p = .036$). There was no significant difference between the two smaller eccentricities (Δsensitivity$_{4\text{–}9}$ = –0.01, 95% CI [–0.13, 0.12], $t(20) = –0.14$, p

= .893). The interaction between memory load and eccentricity did not affect d' ($F(2,40) = 1.00$, $p = .377$).

Also in the perceptual control task, d' was lowest at the largest eccentricity of 14 dva (**Figure S11**). We corroborated this finding using a two-way rmANOVA and observed a significant main effect of eccentricity ($F(2,40) = 5.91$, $p = .006$). Post-hoc *t*-tests revealed lower sensitivity at 14 dva ($M = 1.49$, $SD = 0.18$, 95% CI [1.44, 1.54]) as compared to 9 dva ($M = 1.63$, $SD = 0.16$, 95% CI [1.58, 1.67]; $\Delta\text{sensitivity}_{9\text{–}14} = 0.13$, 95% CI [0.04, 0.23], $t(20) = 2.91$, $p = .009$) and 4 dva ($M = 1.61$, $SD = 0.15$, 95% CI [1.57, 1.66]; $\Delta\text{sensitivity}_{4\text{–}14} = 0.12$, 95% CI [0.03, 0.21], $t(20) = 2.82$, $p = .011$). Sensitivity did not differ significantly between the two smaller eccentricities ($\Delta\text{sensitivity}_{4\text{–}9} = -0.01$, 95% CI [–0.10, 0.07], $t(20) = -0.32$, $p = .752$). Neither the number of stimuli (low memory load: $M = 1.59$, $SD = 0.20$, 95% CI [1.53, 1.65]; high memory load: $M = 1.56$, $SD = 0.14$, 95% CI [1.51, 1.62]; $F(1,20) = 0.29$, $p = .597$) nor the interaction with eccentricity significantly influenced sensitivity in the perceptual task ($F(2,40) = 2.73$, $p = .077$).

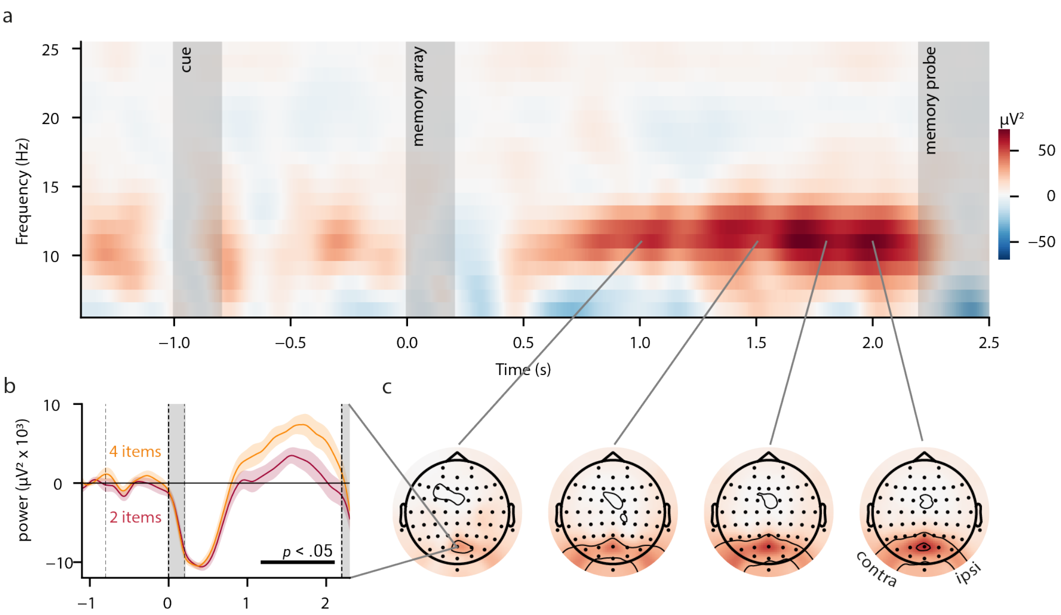

Figure S11: Effect of memory load on global (i.e., non-lateralized) alpha power. Some previous studies have found that non-lateralized alpha power is modulated by memory load (Pavlov & Kotchoubey, 2022). In an exploratory analysis, we checked whether this effect is also present in our data. (a) shows a time-frequency decomposition averaged across all EEG channels (normalized by subtracting the mean power during a baseline window 300–100 ms before cue onset). During the retention interval we observed an increase in power in the alpha frequency range which was most prominent in parieto-occipital sensors along the midline (c). For electrode POz (chosen by visual inspection of these topographies), we found that this effect was stronger for the high than for the low memory load condition (b). This was corroborated by a cluster-corrected *t*-tests comparing the alpha power values (high vs low memory load) in channel POz during the retention interval, which yielded one significant cluster (1,168–2,108 ms after onset of the memory array; black line). To test whether this effect was further modulated by stimulus eccentricity, we modeled the average signal within the significant cluster with a rmANOVA (factors: memory load, eccentricity). We did not find a significant main effect of eccentricity ($F(2,40) = 2.32$, $p = .112$) nor for its interaction with memory load ($F(2,40) = 2.70$, $p = .080$). The significant main effect of memory load ($F(1,20) = 4.51$, *p* = .046) just confirmed the result of the cluster-based permutation test which guided the selection of the time-window.

References:

Bates, D., Mächler, M., Bolker, B., & Walker, S. (2015). Fitting Linear Mixed-Effects Models Using lme4. *Journal of Statistical Software*, *67*, 1–48. https://doi.org/10.18637/jss.v067.i01

Hakim, N., Adam, K. C. S., Gunseli, E., Awh, E., & Vogel, E. K. (2019). Dissecting the Neural Focus of Attention Reveals Distinct Processes for Spatial Attention and Object-Based Storage in Visual Working Memory. *Psychological Science*, *30*(4), 526–540. https://doi.org/10.1177/0956797619830384

Haufe, S., Meinecke, F., Görgen, K., Dähne, S., Haynes, J.-D., Blankertz, B., & Bießmann, F. (2014). On the interpretation of weight vectors of linear models in multivariate neuroimaging. *NeuroImage*, *87*, 96–110. https://doi.org/10.1016/j.neuroimage.2013.10.067

Jas, M., Engemann, D. A., Bekhti, Y., Raimondo, F., & Gramfort, A. (2017). Autoreject: Automated artifact rejection for MEG and EEG data. *NeuroImage*, *159*, 417–429. https://doi.org/10.1016/j.neuroimage.2017.06.030

Keefe, J. M., & Störmer, V. S. (2021). Lateralized alpha activity and slow potential shifts over visual cortex track the time course of both endogenous and exogenous orienting of attention. *NeuroImage*, *225*, 117495. https://doi.org/10.1016/j.neuroimage.2020.117495

Livingstone, A., Christie, G., Wright, R., & McDonald, J. (2017). Signal Enhancement, Not Active Suppression, Follows the Contingent Capture of Visual Attention. *Journal of Experimental Psychology: Human Perception and Performance*, *43*, 219–224. https://doi.org/10.1037/xhp0000339

Pavlov, Y. G., & Kotchoubey, B. (2022). Oscillatory brain activity and maintenance of verbal and visual working memory: A systematic review. *Psychophysiology*, *59*(5), e13735. https://doi.org/10.1111/psyp.13735